Naval Research Laboratory

Washington, DC 20375-5320

NRL/MR/5650--05-8851

Overview of Microring Resonators with Applications to a Tunable Bandpass Filter

PATRICK F. KNAPP

SFA, Inc.
Largo, MD

MATTHEW S. ROGGE

Photonics Technology Branch
Optical Sciences Division

March 4, 2005

REPORT DOCUMENTATION PAGE

Form Approved
OMB No. 0704-0188

1. REPORT DATE *(DD-MM-YYYY)*	2. REPORT TYPE	3. DATES COVERED *(From - To)*
04-03-2005	Memorandum	August 2004-November 2004

4. TITLE AND SUBTITLE

Overview of Microring with Applications to a Tunable Bandpass Filter

5a. CONTRACT NUMBER
2525

5b. GRANT NUMBER

5c. PROGRAM ELEMENT NUMBER

6. AUTHOR(S)

Patrick F. Knapp* and Matthew S. Rogge

5d. PROJECT NUMBER

5e. TASK NUMBER

5f. WORK UNIT NUMBER

7. PERFORMING ORGANIZATION NAME(S) AND ADDRESS(ES)

Naval Research Laboratory, Code 5650
4555 Overlook Avenue, SW
Washington, DC 20375-5320

8. PERFORMING ORGANIZATION REPORT NUMBER

NRL/MR/5650--05-8851

9. SPONSORING / MONITORING AGENCY NAME(S) AND ADDRESS(ES)

Naval Research Laboratory, Code 5650
4555 Overlook Avenue, SW
Washington, DC 20375-5320

10. SPONSOR / MONITOR'S ACRONYM(S)

11. SPONSOR / MONITOR'S REPORT NUMBER(S)

12. DISTRIBUTION / AVAILABILITY STATEMENT

Approved for public release; distribution is unlimited.

13. SUPPLEMENTARY NOTES

*SFA, Inc., 9315 Largo Drive West, Suite 200, Largo, MD 20774

14. ABSTRACT

We give here a detailed description of the operation of a microring resonator, including a mathematical derivation of the filter response for first order elements and analysis of higher order elements. We show that the operation is analogous to that of a Fabry-Perot resonator. We then describe the tunable bandpass filter made by Little Optics (LO). We discuss its architecture and specifications. Finally, data taken of the LO filter is shown and analyzed, concluding that the LO BPF has excellent out-of-band rejection, but in wideband applications it would perform poorly due to spurious peaks in the wideband filter response.

15. SUBJECT TERMS

BPF (bandpass filter); Microring; Resonator

16. SECURITY CLASSIFICATION OF:			17. LIMITATION OF ABSTRACT	18. NUMBER OF PAGES	19a. NAME OF RESPONSIBLE PERSON
a. REPORT	b. ABSTRACT	c. THIS PAGE			Patrick F. Knapp
Unclassified	Unclassified	Unclassified	UL	17	19b. TELEPHONE NUMBER *(include area code)* (202) 767-9553

Standard Form 298 (Rev. 8-98)
Prescribed by ANSI Std. Z39.18

CONTENTS

OVERVIEW OF MICRORING RESONATORS WITH APPLICATIONS TO A TUNABLE BANDPASS FILTER

Executive Summary

- The microring resonator is a tunable, narrow-bandwidth optical filter. In this report we analyze i) the general operating principles of microring resonators and ii) the performance of a specific filter manufactured by Little-Optics, Inc. (Annapolis Junction, MD).

- The Little Optics filter has a 3-dB spectral width of approximately 32 GHz and is tunable by computer control over a wavelength range of 40 nm. The filter is also characterized by relatively flat passband and insertion loss of 5.5 dB.

- The filter employs multiple stages, called "Vernier" stages, to significantly increase free-spectral range and polarization diversity to relax manufacturing tolerances imposed by polarization dependencies.

- Although the filter exhibits extraordinarily high out-of-band suppression (>80db optical) near the passband, imperfections in the Vernier and polarization diversity stages allow spurious peaks to appear in the frequency response thus limiting the usefulness of the device in wideband or channelization applications.

Manuscript approved November 24, 2004.

I. Introduction:

This report documents the basic operation and principles of an optical microring resonator as well as the architecture and structure of the Little Optics[1] Tunable Band Pass Filter (LO BPF). It is intended to give a basic understanding of the physical and mathematical mechanisms at work in a microring resonator and provide a basis for judging the design and operation of a microring based filter. This report will begin with the physical structure and operation of a 1st order microring add/drop filter, and move on to higher order structures and finally, will present a short analysis of the design and operation of the LO BPF.

II. Operation of a Single Ring (1st order structures):

Basics:

A microring filter consists simply of two bus waveguides (input and output) with a ring waveguide situated in between. Each waveguide is coupled to the ring either vertically or laterally. In lateral coupling, the less efficient of the two methods, the waveguides lie in the same plane as the ring, while in vertical coupling the ring is seated above the two waveguides. Because Little Optics employs vertical coupling in its filter design we will focus exclusively on vertically coupled microring resonators [1]. Figure 1 shows a vertically coupled ring resonator. The light is coupled between waveguides via evanescent field coupling, and the amount of energy coupled from one waveguide to another is denoted by a coupling coefficient. The dominating parameter controlling the coupling coefficients between the buses and the ring is the separation between the two waveguides (t_s). Therefore, in a vertical coupling scheme the coupling coefficient is controlled by varying the height of the layer separating the ring from the bus. Because this height can be precisely controlled, by growing a separation layer in between the ring and bus layers, the coupling coefficient can also be precisely controlled. This sole fact makes vertically coupled resonators far easier to manufacture than laterally coupled ones.

[1] Little Optics, Inc., 9020 Junction Drive, Annapolis Junction, MD 20701

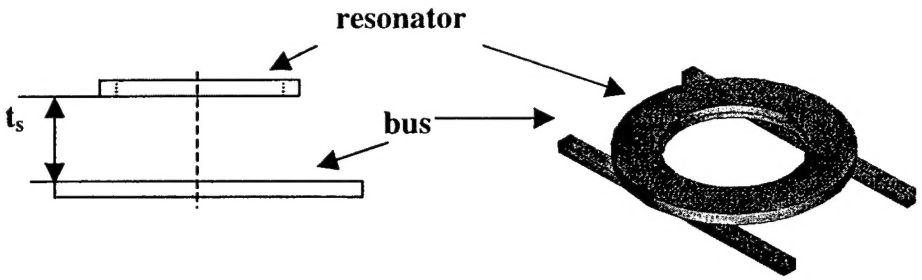

Fig 1: Diagrams of a vertically coupled microring resonator

Relevant Parameters:

As stated above, the coupling coefficients are controlled primarily by the height, t_s, of the separation layer between the ring and the bus. There are three main coupling coefficients that affect the performance of the resonator. These three coefficients denote 1) the field amplitude coupled from the bus to the ring while traveling through the coupling region, 2) the field amplitude coupled from the ring to the bus while traveling through the coupling region and finally 3) the field amplitude remaining in the ring after the wave has passed a coupling region. These three parameters are important in obtaining the overall response of the filter and greatly affect the Q factor, finesse and insertion loss.

Another important factor in determining a ring resonator's response is the effective ring radius ($\mathbf{R_{eff}}$). Light traveling through a ring will not follow a narrow path around the ring. Instead its path will be distributed radially from the center of the ring. This distribution is due in large part to the distribution of the light incident on the ring. However, waves in the ring are scattered as they propagate due to reflections from the walls, which causes further distortion of the light's distribution. The radial distance from the center of the ring to the centroid of this distribution is known as the effective ring radius or $\mathbf{R_{eff}}$ [2]. Changing the radii of the ring and the index contrast between the waveguide and the cladding can vary $\mathbf{R_{eff}}$. Changing these factors will change how light scatters in the ring and how well it is confined. $\mathbf{R_{eff}}$ is the primary factor determining the resonance wavelength of a ring.

Finally, the propagation losses in the ring contribute to the overall filter response, affecting the Q factor, finesse and insertion loss. Relevant losses are substrate leakage loss, bending loss and surface scattering loss. Scattering losses can be

minimized by improving manufacturing processes and realizing smoother waveguide walls. However, bending and leakage losses are closely tied to the ring radius and index contrast, respectively. Therefore, tradeoffs must be made when designing a ring resonator to minimize losses while simultaneously maximizing other factors such as coupling and tuning range.

Determining Filter Response:

Now that we know what parameters are relevant to the operation of a ring resonator we can begin to understand how they work. A microring is nothing more than a cavity that circulates light, letting part of the light escape after each round trip. With this understanding, it is obvious that a microring operates much like a Fabry-Perot resonator [2]. In a Fabry-Perot resonator two semi reflective mirrors are positioned parallel to one another forming a cavity. Light is allowed to enter only through one side of the cavity and exit the other. The light is then circulated between the two mirrors and after each round trip some light is allowed to escape the cavity. The amount of light that remains in the cavity and the amount that escapes are governed by the reflectivities of the front and rear mirrors, $\mathbf{r_1}$ and $\mathbf{r_2}$ respectively. After each pass in the cavity, the output light has a phase determined by its wavelength and the length of the cavity. For resonant wavelengths, the phase difference between the subsequent passes is an integer multiple of 2π and the light constructively adds. Other wavelengths suffer some degree of destructive interference and exit the system significantly more attenuated.

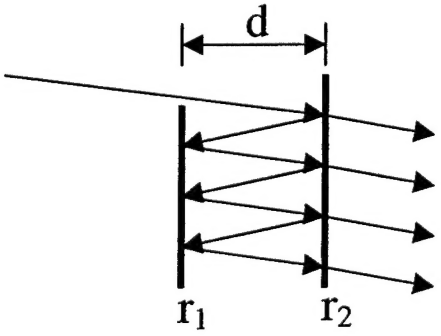

Fig 2: Diagram of a Fabry-Perot cavity

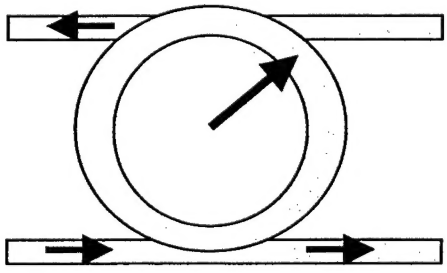

Fig. 3: illustration of a ring resonator

Looking at the ring in this way, it becomes clear that the coupling coefficients of the microring resonator are analogous to the mirror reflectivities because they determine how much light enters the ring, how much light stays in the ring after every pass and how much light exits the ring on every pass. Furthermore, the effective circumference of the ring ($2\pi\mathbf{R}_{\mathbf{eff}}$) determines the round trip phase shift of a wave traveling through the ring. Mathematically, the response can be computed by entering a field into the ring and computing how much of it leaves the ring and how much of it is transmitted after each pass of the coupling region. This is accomplished simply by multiplying the field by the proper coupling coefficients. In addition, the phase shift experienced by the wave must be accumulated at each pass around the ring. The process starts with an incident field E entering the input waveguide.

$$E = E_o e^{-j\omega t} \tag{1}$$

A portion of E is coupled from the bus waveguide to the ring. This is expressed by multiplying E by the coupling coefficient $\mathbf{a}_{\mathbf{br}}$. Then, the wave travels halfway around the ring, experiencing a phase shift proportional to half the circumference of the ring and loss due to propagation. At the coupling region between the output waveguide and the ring the field looks like this:

$$E_{r1} = a_{br} \cdot \gamma \cdot e^{-j\theta} \cdot E \tag{2}$$

$$\theta = \frac{\pi R_{eff}\,\omega}{\upsilon} \quad \text{the phase shift due to one half round trip}$$

where υ is the velocity of the wave in the ring and γ is the loss due to one half roundtrip.

The portion of E_{r1} that leaves the ring and is seen at the output is denoted by E_{drop}.

$$E_{drop} = a_{rb} E_{r1} \tag{3}$$

$\mathbf{a}_{\mathbf{rb}}$ denotes the fraction of the field that leaves the ring through the drop port.

The portion of E_{r1} that remains in the ring is denoted by E_r.

$$E_r = b_r E_{r1} \tag{4}$$

E_{drop} is equal to E_{r1} multiplied by the coupling coefficient $\mathbf{a}_{\mathbf{rb}}$, which denotes the amount of field coupled from the ring to the bus waveguide. Whereas, E_r is equal to E_{r1} multiplied by the coupling coefficient $\mathbf{b}_{\mathbf{r}}$, which denotes the fraction of the field

amplitude that stays in the ring after passing the coupling region. We continue tracking E_r to determine the effect of multiple passes around the ring on the wave inside.

At the output after the next trip

$$E_{drop} = a_{br} \cdot a_{rb} \cdot b_r^{\,2} \cdot \gamma^3 e^{-j3\theta} \cdot E \tag{5}$$

$$E_r = a_{br} \cdot b_r^{\,3} \cdot \gamma^3 e^{-j3\theta} \cdot E \tag{6}$$

After the third trip

$$E_{drop} = a_{br} \cdot a_{rb} \cdot b_r^{\,4} \cdot \gamma^5 \cdot e^{-j5\theta} \cdot E \tag{7}$$

$$E_r = a_{br} \cdot b_r^{\,5} \cdot \gamma^5 \cdot e^{-j5\theta} \cdot E \tag{8}$$

Completing three iterations is sufficient to see the pattern emerging. Taking successive E_{drop} terms and looking more closely at them, it is evident that they can be written as a geometric series, the sum of which is of the form

$$s = \sum_{n=0}^{\infty} a \cdot r^n \tag{9}$$

We are interested in the sum because the filter response is the compound effect the ring has on the wave as the number of round trips approaches infinity. The sum of the Edrop terms as the number of iterations approaches infinity is as follows.

$$\sum_{n=1}^{\infty} E_{drop}(n) = \sum_{n=1}^{\infty} a_{rb} a_{br} \gamma^{2n-1} e^{-j\theta(2n-1)} b_r^{\,2n-2} E \tag{10}$$

This sum can be made to look like the sum of a geometric series

$$\sum_{n=1}^{\infty} E_{drop}(n) = a_{rb} a_{br} \gamma \cdot e^{-j\theta} \cdot E \cdot \sum_{n=1}^{\infty} \gamma^{2n-2} e^{-j\theta(2n-2)} b_r^{\,2n-2} \tag{11}$$

$$\sum_{n=1}^{\infty} E_{drop}(n) = a_{rb} a_{br} \gamma \cdot e^{-j\theta} \cdot E \cdot \sum_{n=1}^{\infty} (\gamma^2 e^{-j2\theta} b_r^{\,2})^{n-1} \tag{12}$$

substituting n = m+1, we have

$$\sum_{m=0}^{\infty} E_{drop}(m+1) = a_{rb} a_{br} \gamma \cdot e^{-j\theta} \cdot E \cdot \sum_{m=0}^{\infty} (\gamma^2 e^{-j2\theta} b_r^{\,2})^{m}$$

The sum of a geometric series can be written as

$$s = \frac{a}{1-r}, r < 1 \tag{13}$$

Where, in this case

$$a = a_{rb}a_{br}\gamma \cdot e^{-j\theta} \cdot E, \qquad r = b_r{}^2\gamma^2 e^{-j2\theta} \tag{14}$$

it can be shown that $r = b_r{}^2\gamma^2 e^{-j2\theta}$ is always less than one because b_r and γ are both fractions less than one and the magnitude of $e^{-j2\theta}$ is always equal to one. Therefore, the total filter response, E_{drop}, is equal to the sum of the geometric series, which, after substituting in for E and θ, looks like this

$$E_{drop} = \frac{E_o \cdot a_{br} \cdot a_{rb} \cdot \gamma \cdot e^{-j\omega t} \cdot e^{\frac{-j\pi R_{eff}\omega}{v}}}{1 - b_r{}^2\gamma^2 e^{\frac{-j2\pi R_{eff}\omega}{v}}} \tag{15}$$

The suppression of the filter can be written as shown in equation (16) below. The frequency dependence has been converted to wavelength for simplicity and the $e^{-j\omega t}$ term has been removed because its magnitude is one.

$$\frac{E_{drop}}{E_o} = \left(\frac{a_{br} \cdot a_{rb} \cdot \gamma \cdot e^{-\left(\frac{j\cdot 2\cdot \pi^2 \cdot R_{eff}}{\lambda}\right)}}{1 - b_r{}^2 \cdot \gamma \cdot e^{-\left(\frac{j4\cdot \pi^2 \cdot R_{eff}}{\lambda}\right)}} \right) \tag{16}$$

The above equation is the derived filter response of the resonator where E_{drop} is the field amplitude at the drop port of the ring, E_o is the input field amplitude, $\mathbf{a_{br}}$ is the fraction of amplitude coupled from the bus waveguide to the ring, $\mathbf{a_{rb}}$ is the fraction of amplitude coupled from the ring to the output bus waveguide, $\mathbf{b_r}$ is the fraction of amplitude transmitted in the ring when passing the coupling region and $\boldsymbol{\gamma}$ represents the different losses in the ring due to one half round trip.

III. Higher Order Structures:

Higher order structures can be modeled as cascaded first order elements. This allows for simple analysis of higher order structures once the first order problem has been solved. Higher order microring resonators allow for much steeper roll off than their first order counter parts. This provides the user with much greater filtering precision. The downside to using higher order elements is that all the rings in a multi-order resonator must be made identical and tuned identically. This increases the filter's dependencies on manufacturing errors. Multi-order resonators also take up more space and introduce more propagation losses to the system.

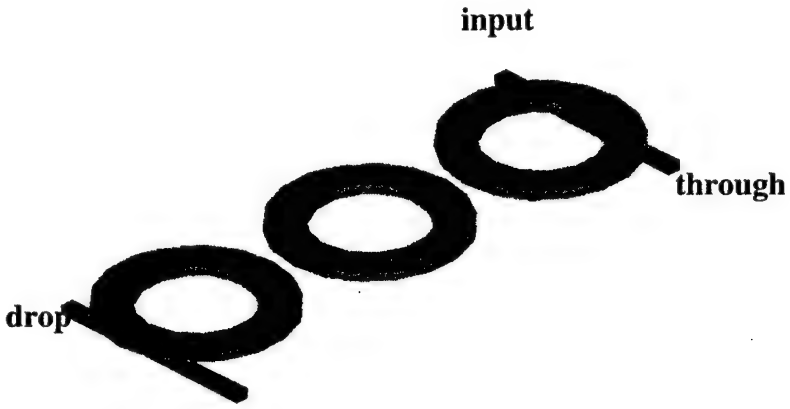

Fig 5: A 3rd order vertically coupled microring resonator. The rings are laterally coupled to one another.

Using equation 12 we simulated the filter operation for first and third order elements. The third order structures were simulated by cascading three first order filters; this was mathematically realized by multiplying their responses. Figure 6 shows the simulation results.

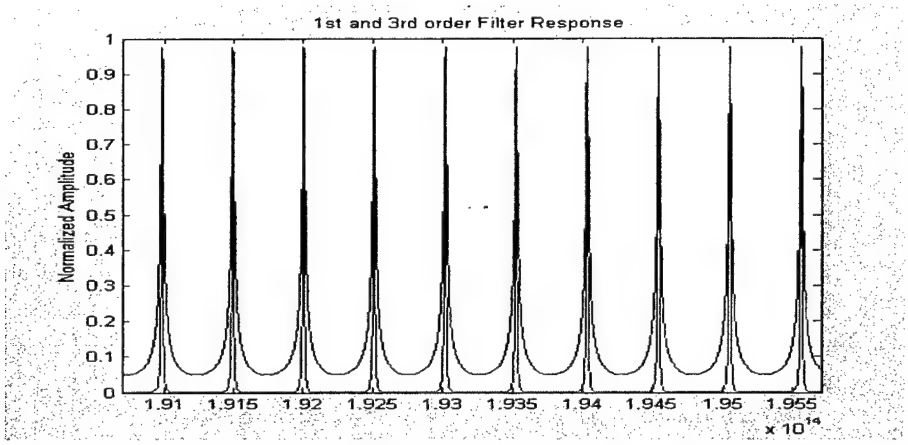

Figure 6: Simulation results for first and third order microring resonators.

Clearly, the third order filter has a much sharper response, resulting in greater suppression and narrower BW. Therefore, with minimal addition of cost or parts, because the rings are all etched simultaneously, the performance of a microring structure can be vastly improved by going to a higher order. The one downside is that the signal experiences increasing insertion loss as the order is increased. This can be minimized, but not overcome, by minimizing the losses in the rings.

IV. Little Optics Design and Architecture:

Currently, Little Optics employs either 3rd or 5th order resonators in their tunable BPF's. This means that three or five rings construct one cavity, with bus waveguides coupled to the outer rings only. The bus waveguides are still vertically coupled to the outer rings, but the rings are laterally coupled to each other. This is done so that all of the rings can be etched on the same layer, making it easier to create identical rings. In addition, having all the rings on the same layer makes it easy to tune them simultaneously and identically. Figure 5 above shows a drawing of a 3rd order resonator used by Little Optics.

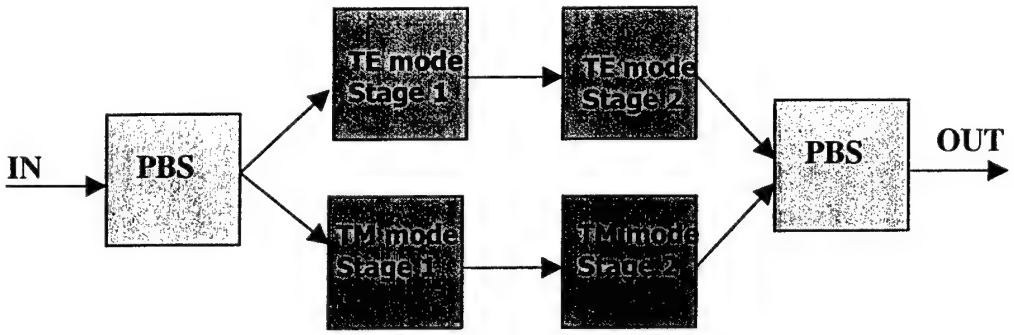

Figure 7: Block Diagram of the Little Optics Tunable BPF

Little Optics employs two unique aspects in their design. They are shown in the schematic in figure 7. First is a Vernier architecture, which is used to increase the FSR of the filter. This is done by connecting two 3rd or 5th order resonators with different FSR's in series. The first resonator puts up a comb of resonance wavelengths. The second resonator is tuned to select just one resonance and suppress the others. In the case of the current BPFs by Little Optics, the first resonator has an FSR of approximately 575 GHz, and the second has an FSR of approximately 650 GHz. The composite response of these two filters yields an FSR of about 4.9 THz. The previous simulation was again used to recreate the effects of the Vernier configuration. This was accomplished by creating two filters with different FSR's and cascading their responses. The results are shown in figure 8 below. The results of the Vernier configuration are not ideal, and lead to spurious side peaks.

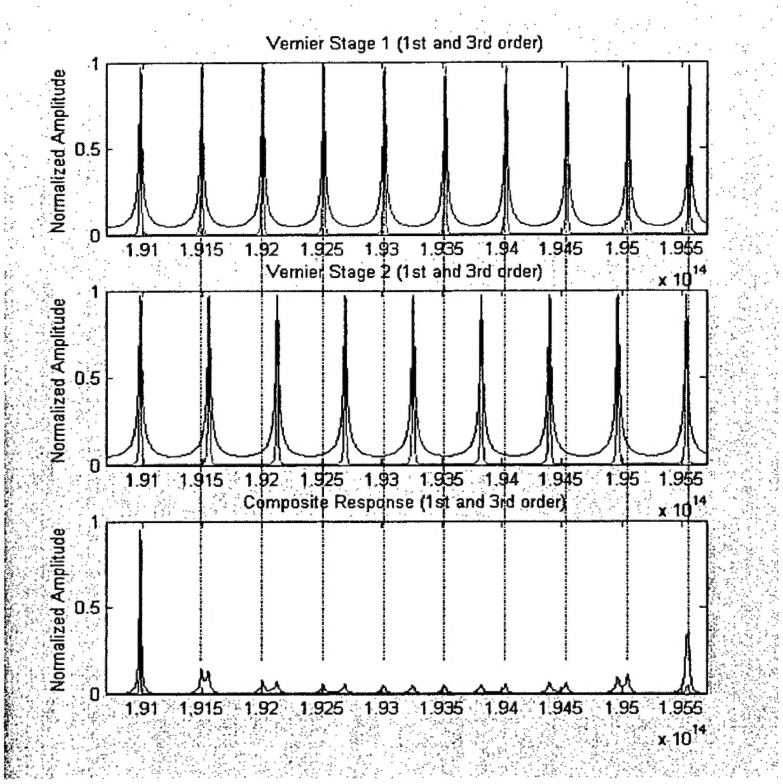

Figure 8: The top two plots show the responses of each stage independently. The third plot shows the result of cascading the first two responses. Dashed lines are used to show offset of peaks from each stage

The second unique design feature is use of Polarization Beam Splitting (PBS) to process TE and TM waves separately, a common polarization diversity technique. This is done to relax manufacturing tolerances on the rings. TE and TM polarized waves respond differently to the same ring, so the different polarizations are branched off and processed by rings tuned to TE and TM light respectively. Each branch results in the same resonance wavelength and are recombined at the output to reform the wave.

V. Performance of the Little Optics BPF:

The filter tested displays steep roll off and a fairly flat pass band. It offers an astonishing 80dB suppression immediately out of the pass band. The filter experimentally matches factory specifications on most parameters and is consistent with available data. The table below shows the measured parameters compared to the factory specifications. Its large suppression and steep roll off make this filter very

attractive and promising, but there are several weak points in the filter's response that severely degrade its overall performance.

Parameter	Spec	Measured
Channel Spacing (GHz)	50	57
Tuning Range (nm)	40	Not tested
0.5 dB BW (GHz)	> 20	20.97
3 dB BW (GHz)	N/A	31.95
30 dB BW (GHz)	< 90	69.64
Adj. Channel crosstalk (dB)	> 30	~12.5
IL (dB)	< 5.5	5.3

Table 1: factory specified parameters compared to measured device parameters

The Vernier architecture accomplishes its goal of increasing the FSR, but introduces some additional adverse affects. In real world operation the second filter does not suppress all of the FSR peaks of the first filter, nor does the first suppress the peaks of the second. Instead, pairs of peaks appear to the left and right of the main resonance peak. These spurious peaks are not as high as the main peak, but appear, in the worst case, 30 dB down from the main peak. The detrimental effect of these peaks can be seen in figure 9 below. This is a plot of data taken for the Little Optics filter.

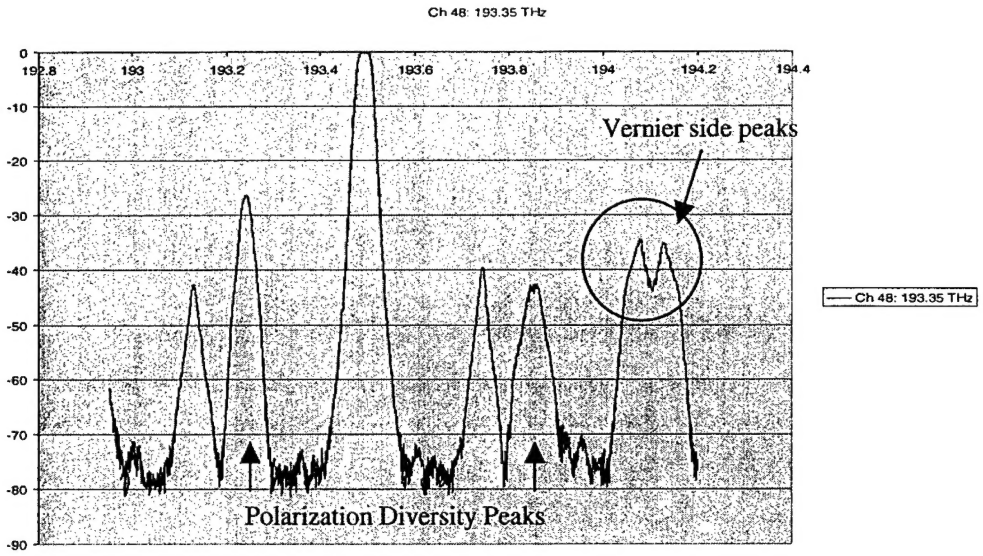

Figure 9: experimentally acquired filter response. Data taken at the NRL

x-axis is in THz, y-axis in dBm

In addition, the Polarization Beam Splitting technique has a similar adverse affect. Since the beam splitters are not perfect, TE light is allowed to travel through the TM branch and vice versa. The result is that the TE light sees a different resonance than the TM does, and therefore a new peak appears offset from the main one. The same happens to the TM light traveling through the TE branch. In all, two spurious peaks appear immediately to the left and right of the main peak due to non-ideal Polarization Beam Splitting. These peaks appear at their worst 25dB down from the main peak. Again, this affect severely degrades the wideband performance of this filter and can be seen in figure 9.

VI. Conclusion:

Microring resonators are a unique and promising filtering technology. Their compact size and ideal response show potential for optical integrated circuitry. The major obstacle left is to perfect the manufacturing processes of the rings. Optimizing the manufacturing processes will allow for better filter shapes, lower loss and smaller size.

The Little Optics filter demonstrates the potential of the resonator technology while simultaneously showing the shortcomings of their real world implementation. The tunable BPF demonstrates a steep and narrow response with unprecedented out of band rejection, making it ideal for some precise filtering applications. But, the adverse effects of the polarization beam splitting and Vernier architecture will ultimately limit the performance in wideband applications.

Acknowledgements:

The author acknowledges helpful discussions with Frank Bucholtz.

References:

1) Andrin Stump; Jens Kunde; Ulrich Gubler; Anne-Claire Pliska-Leduff; Christian Bosshard, "A study on a microring structure for practical devices," Optical and Quantum Electronics, vol. 35, Issue 13, pp. 1205-1213, Oct 2003.

2) M.K. Chin, S.T Ho, "Design and modeling of waveguide-coupled single-mode microring resonators," Journal of Lightwave Technology, vol. 16, issue 8, pp. 1433-1446, Aug. 1998.